Talanta 195 (2019) xxx–xxx

Contents lists available at ScienceDirect

Talanta

journal homepage: www.elsevier.com/locate/talanta

Impedimetric sensor for tyramine based on gold nanoparticle doped-poly (8-anilino-1-naphthalene sulphonic acid) modified gold electrodes

Wanderson da Silva[a], Mariana Emilia Ghica[a], Rachel F. Ajayi[b], Emmanuel I. Iwuoha[b], Christopher M.A. Brett[a,*]

[a] Department of Chemistry, Faculty of Sciences and Technology, University of Coimbra, 3004-535 Coimbra, Portugal
[b] SensorLab, Department of Chemistry, University of Western Cape, 7535 Bellville, Cape Town, South Africa

ARTICLE INFO

Keywords:
Tyramine
Biogenic amine
Food safety control
Electrochemical impedance detection
Impedimetric sensor

ABSTRACT

A novel impedimetric sensor for the determination of tyramine (Tyr), a biogenic amine, on the surface of gold nanoparticle-poly-(8-anilino-1-napthalene sulphonic acid), AuNP-PANSA modified gold electrode (AuE) is presented for the first time. The AuNP were successfully synthesized by a green synthesis method. Their characterization and optimization were conducted using X-ray diffraction, scanning electron microscopy, transmission electron microscopy, electrochemical impedance spectroscopy and cyclic voltammetry. Under optimal conditions, the impedimetric sensor revealed a relatively broad linear range from 0.8 to 80 μM similar to more complex architectures found in the literature and the limit of detection of 0.04 μM was the lowest achieved until now. In order to test the reliability of the proposed method, real sample application studies were conducted using dairy products and fermented drinks. It was found that the sensor presented a good selectivity and recovery. Furthermore, the impedimetric sensor shows good reproducibility, stability, selectivity and very small interferences which augur well for its application in food safety control processes.

1. Introduction

Biogenic amines are usually used as quality markers of foods because of their impact on human health; if present in food at high concentration levels they can cause illnesses, such as hypotension, migraine, and diarrhoea [1–3]. Tyramine (Tyr) is a well-known biogenic amine produced by the decarboxylation of the amino acid tyrosine, which occurs by degradation resulting from microbial activity. It is often found in fermented foods and beverages, meat, fish, seafood and dairy products [4,5]. Tyr is an indirectly acting sympathomimetic amine which releases norepinephrine from a sympathetic nerve ending, and it has been reported that Tyr-containing foods can cause unnatural and toxic effects when ingested in large quantities [5]. Analytical methods for the determination and quantification of Tyr in food samples described in the literature, include high performance liquid chromatography (HPLC), hyphenated with mass spectroscopy detection, high performance capillary electrophoresis (HPCE), mass spectrometry, real-time polymerase chain reaction (real-time-PCR). Electrochemical detection is promising due to its unique characteristics as well as rapid response, low cost, and high sensitivity and specificity [6–11].

Intrinsically conducting polymers (ICPs) are useful materials for applications in electronics, electrochemistry, and sensors [12,13]. Among the ICPs, polyaniline and its derivatives have attracted much attention due to a good combination of properties such as excellent electrical conductivity, ease of preparation, low cost, and sufficiently good stability [14]. Poly-(8-anilino-1-naphthalene sulphonic acid) (PANSA), represents a new class of ICPs with improved redox activity and conductivity, and is obtained from the oxidation of the bifunctional monomers with -NH_2 and –OH. In both organic and acid media, polymerisation occurs via the amine groups [15]. When the ICPs are combined with other nanostructures such as metallic nanoparticles, the performance of the final nanocomposite can be further improved, since the individual properties of both constituents will be present in the new material configuration. In particular, attachment or incorporation of gold nanoparticles (AuNP) into such polymer films enhances the electron transfer between the redox centres and electrode surfaces making the nanocomposite ideal for sensor applications [16–18].

In this work, a novel and simple preparation method has been developed for the construction of the first sensitive impedimetric sensor based on gold nanoparticle doped-PANSA on a gold substrate for detection of Tyr. Previous work dealt with the development of an

* Corresponding author.
E-mail address: cbrett@ci.uc.pt (C.M.A. Brett).

https://doi.org/10.1016/j.talanta.2018.11.054
Received 31 July 2018; Received in revised form 9 November 2018; Accepted 19 November 2018
Available online 22 November 2018
0039-9140/ © 2018 Elsevier B.V. All rights reserved.

amperometric biosensor for Tyr using tyrosinase on a glassy carbon electrode [19]. Electrochemical deposition of poly-(8-anilino-1-naphthalene sulphonic acid) together with attached AuNP on gold electrodes (AuE) by polymerisation of the monomer and gold nanoparticles aims at developing a sensitive and easily fabricated electrochemical sensor for Tyr detection. The analytical performance of the impedimetric sensor, stability, and selectivity was investigated, together with optimization of parameters that influence Tyr detection, such as applied potential and pH. Finally, the impedimetric sensor was applied to the determination of the Tyr content in food products.

2. Experimental

2.1. Material and reagents

Tyramine, 99%, gold (III) chloride trihydrate ($HAuCl_4{\cdot}3H_2O$), 8-anilino-1-naphthalene sulphonic acid, 97% (ANSA) were purchased from Sigma-Aldrich. For the electrochemical experiments, the Britton-Robinson (BR) buffer supporting electrolyte was prepared by mixing phosphoric acid, acetic acid and boric acid (all solutions of 0.04 M) and adjusting the pH with 0.2 M sodium hydroxide. All reagents were of analytical grade and were used without further purification.

Millipore Milli-Q nanopure water (resistivity $\geq$ 18 MΩ cm) was used for the preparation of all solutions. All experiments were performed at room temperature (25 ± 1 °C).

2.2. Instrumentation and methods

A gold electrode (AuE) (geometric area 0.00785 cm^2) or AuE modified with AuNP, PANSA or AuNP-PANSA was used as working electrode, a platinum wire as counter electrode and an Ag/AgCl (3 M KCl) electrode as reference. Voltammetric experiments were performed using an Ivium CompactStat potentiostat (Ivium Technologies, Utrecht, Netherlands). Electrochemical impedance measurements were carried out with a Solartron 1250 Frequency Response Analyser coupled to a Solartron 1286 electrochemical interface using ZPlot 2.4 software (Solartron Analytical, UK). A sinusoidal voltage perturbation of amplitude 10 mV rms was applied in the frequency range between 65 kHz and 0.1 Hz with 10 frequency steps per decade. The pH measurements were carried out using a glass electrode pH meter model Crison Micro pH 2001 (Crison Instruments, S.A., Barcelona, Spain) at room temperature. The XRD studies were carried out with an X-ray powder diffraction system (Siemens D5000, Bruker-AXS, Karlsruhe, Germany), Cu-Ka radiation (($\lambda K\alpha_1$ = 1.5406 Å) in the 2θ range available, 0.5–130°, with a voltage of 40 kV and current 40 mA. Scanning electron microscopy (SEM) (model JSM-5310, JEOL, Co., Japan) was used for the characterization of the AuNP and the morphology of the polymer and nanocomposite films.

2.3. Synthesis of gold nanoparticles (AuNP)

AuNP were made by a green synthesis method by the addition of purified juice of *C. sinensis* [20]. Squeezing was used to extract approximately 10 mL of the juice, which was then strained through a fine-mesh sieve to separate the solid parts from the liquid. The liquid extract was centrifuged at 14,000 rpm for 30 min to remove all undesired material in suspension and leave a clear solution. A volume of 50 mL of a solution containing 1 mM of $HAuCl_4{\cdot}3H_2O$ was brought to the boil on a hot plate with constant stirring, and then 5 mL of the purified liquid extract from *C. sinensis* was added. The hot plate was then turned off but stirring was continued for 5 min until the colour change from yellow to colourless and finally to intense red. This colloidal solution was centrifuged at 14,000 rpm for 20 min to precipitate the gold nanoparticles. The solid was then re-dispersed in 50 mL of Milli-Q water, resulting a concentration of 197 mg L^{-1} for the gold nanoparticles.

2.4. Preparation of the modified electrodes

The PANSA and AuNP-PANSA films were prepared by electrochemical polymerisation of ANSA on the AuE from a solution containing 0.1 M of the ANSA monomer in 0.5 M H_2SO_4; in the latter case, the solution also contained a previously prepared colloidal solution of AuNP which was added to the solution of the corresponding monomer in the volume ratio 1:3 (v/v), leading to a dilution of ANSA monomer to 0.075 M. The mixture was sonicated for 5 min in order to guarantee a better homogeneity and a good dispersion of the AuNP in solution. Solutions were degassed with N_2 for 20 min and the polymer grown on AuE by potential cycling in the range 0.0–1.1 V vs Ag/AgCl at a scan rate of 50 mV s^{-1} for seven cycles. An N_2 blanket was maintained on top of the cell solution during the polymerisation process [14]. AuE was also modified with only AuNP by drop casting 2 μL of the colloidal solution on the electrode substrate.

Similar PANSA and AuNP-PANSA films were prepared on carbon film electrodes in order to use for the characterization by SEM.

The modified electrodes were left to dry at room temperature before further use.

2.5. Sample preparation

In order to evaluate the practical application of the proposed method, AuNP-PANSA/AuE was used to determine Tyr in dairy products and fermented drinks, obtained commercially in a local supermarket. Sample preparation is described below.

A yogurt sample of 2.5 g was accurately weighed and diluted in 20 mL of 0.1 M BR buffer (pH 7.0). The same quantity of Roquefort cheese was weighed and treated in a similar way by adding the same amount of buffer; it was then homogenized until obtaining a milky-looking solution. Yogurt and cheese dispersions were centrifuged at 14,000 rpm for 20 min and the supernatant collected and stored at 4 °C before use.

A volume of 200 μL of Pilsen-type beer was degassed in an ultrasonic bath for 10 min in order to eliminate the gas and avoid the excessive formation of foam during manipulation and analysis which may compromise the measurements.

The wine did not require any kind of preparation and was used as received without pre-treatment.

3. Results and discussion

3.1. Preparation of poly(8-anilino-1-naphthalene sulphonic acid) (PANSA/AuE) and gold nanoparticle doped-poly(8-anilino-1-naphthalene sulphonic acid) (AuNP-PANSA/AuE)

Fig. 1A and B show cyclic voltammograms (CV) corresponding to the formation of PANSA and the nanocomposite AuNP-PANSA films, respectively, on the gold electrode during 7 potential cycles. The good growth of both polymer film and nanocomposite was successful as seen from the well-defined voltammograms and increases in current in successive cycles. Both PANSA and AuNP-PANSA present one redox couple, the associated peak currents for growth of AuNP-PANSA being lower than of PANSA. This can be attributed to the lower monomer concentration after addition of the gold nanoparticle solution. The ANSA was polymerised from a solution of 0.1 M ANSA, whilst the AuNP-PANSA was made from 0.075 M ANSA. The rate of polymerisation was also slightly different. The deposition was very fast at the beginning for PANSA and then slowed down while for AuNP-PANSA the deposition rate is almost constant during the entire polymerisation process, which could be attributed to easier diffusion of monomer in solution at lower concentration. However, even though slightly less polymer is deposited and the rate of deposition changed, the aggregation of the AuNP compensates it, which leads to a higher electrochemical response. Furthermore, as will be seen below, this did not

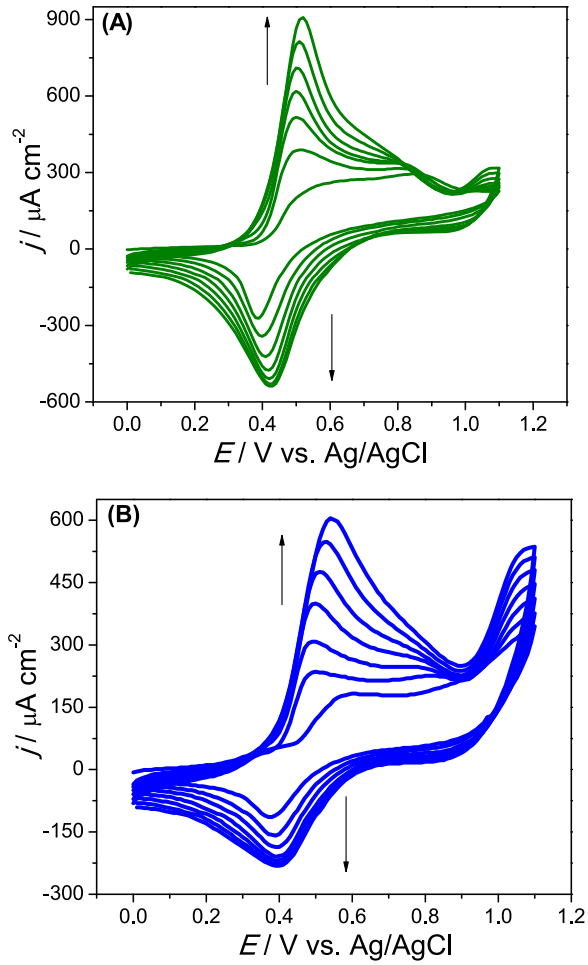

Fig. 1. Electrochemical synthesis of (A) PANSA in 0.1 M ANSA and (B) AuNP-PANSA in 0.075 M ANSA in 0.5 M H_2SO_4 on gold electrodes; scan rate 50 mV s^{-1}.

affect the good performance of the nanocomposite. The midpoint potential between the anodic and cathodic peaks is almost constant: $E_{mid,PANSA} \approx 465$ mV and $E_{mid,AuNP\text{-}PANSA} \approx 450$ mV. The anodic and cathodic peaks increased in height in each of the first 5 cycles indicating successful electrodeposition. However, after the 5th cycle, the cathodic peaks begin to decrease in height while the anodic peaks shift slightly to more positive values with an increasingly slower rate of electrodeposition. This has been attributed to the steric and inductive effect of the naphthalene sulphonic acid moiety [14,21]. There is also an increase in peak separation for both PANSA and AuNP-PANSA, indicating less reversible behaviour with increase in film thickness.

3.2. X-ray diffraction of the gold nanoparticles

The colloidal solution of gold nanoparticles was dropped on glass slides and dried in an oven at 60 °C and after subjected to XRD analysis. Gold nanoparticles synthesized from *C. sinensis,* showed Bragg reflection peaks at 36.4°, 44.3°, 64.9°, and 77.8° for 2θ between 30° and 90° which can be indexed to the (111), (200), (220) and (300) planes, see [19], of face-centred cubic gold crystals (JCPDS), 04–0784, evidencing the crystalline nature of the synthesized AuNP. The peak corresponding to the (111) plane is more intense than the others suggesting its predominance on the exposed faces. Similar results were reported by Khademi et al. [22], Khan et al. [23] and Suresh et al. [24] who also synthesized gold nanoparticles by green synthesis methods.

3.3. Scanning electron microscopy (SEM) of the nanostructures

The morphology and size of the biosynthesized AuNP were studied by SEM. A typical SEM image showing the size and the microstructure of the nanoparticles is given in Fig. 2A. Nanoparticles are predominantly homogenous and spherical in shape; with good dispersibility. The synthesis of controlled sized nanoparticles plays an important role since they can improve significantly its electrochemical properties as compared with non-dispersed or non-homogenous nanoparticles. The average size of the AuNP was analysed by ImageJ open source particle analysis software, in which 100 discreet and well-defined nanoparticles were used as sample space. From Gaussian curve fitting obtained from the histogram, Fig. 2B, the average size of the nanoparticles was found to be 18.0 ± 2.6 nm. Fig. 2C and D show SEM micrographs of the PANSA polymer film and AuNP-PANSA nanocomposite film respectively. PANSA exhibits a rough globular-like sponge structure, while the nanocomposite shows a fine and spherical granule like structure. The difference in morphology between the polymer film and the nanocomposite may be attributed to the lower concentration of the monomer after addition of AuNP solution leading to the formation of a smoother layer due to the decrease of the rate of polymer deposition. The nanoparticles attached to the polymer network can also be seen as uniformly-distributed spherical white spots on the polymer film (Fig. 2D). Energy dispersive X-ray spectroscopy (EDS) obtained from a localized area of the nanocomposite film was performed for evaluate its composition, Fig. 2E. The EDS spectrum reveals the presence of carbon (C), nitrogen (N), oxygen (O) and sulphur (S), all present in the structure of the polymer. Two characteristic X-ray peaks of gold (Au) in the spectrum also proved the presence of the AuNP in the nanocomposite. The EDS spectrum confirms that the new methodology for attaching nanoparticles to the polymer network is efficient.

3.4. Electrochemical characterization of modified electrodes

Unmodified and modified AuE with different nanostructured films: gold nanoparticles (AuNP/AuE), polymer (PANSA/AuE) and composite (AuNP-PANSA/AuE) were characterized by cyclic voltammetry (CV) and electrochemical impedance spectroscopy (EIS) in the presence of Tyr.

3.4.1. Cyclic voltammetry

3.4.1.1. Performance for the determination of Tyr. The effect of modifying the electrode surface on the oxidation process of Tyr was evaluated by cyclic voltammetry, as illustrated in Fig. 3. The anodic and cathodic peak current increased significantly with all modifications tested, being the highest at AuNP-PANSA/AuE. The anodic peak potential shifted to more positive value and the cathodic to more negative value being 0.14 V and −0.22 V at AuE, 0.16 V and −0.24 V at AuNP/AuE, 0.18 V and −0.25 V at PANSA/AuE and 0.28 V and −0.27 V at AuNP-PANSA/AuE, indicating a quasi-reversible oxidation process of tyramine at all electrodes. The significant peak current increase that occurs at AuNP-PANSA/AuE indicates a higher available active surface area compared with AuE, AuNP/AuE and PANSA/AuE. There is also a large increase in the background current at AuNP-PANSA/AuE, which can be attributed to the efficient aggregation of AuNP on the polymer network. AuNP-PANSA/AuE is clearly superior to the other electrode configurations and was chosen to be used in all further studies.

3.4.1.2. Dependence of the oxidation process on the scan rate. The influence of scan rate on the sensor voltammetric response was investigated to ascertain whether it is a diffusion-controlled or a surface-confined process. CVs were recorded at AuNP-PANSA/AuE for 200 µM Tyr in 0.1 M BR buffer pH 7.0 solution at scan rates from 10 to 100 mV s^{-1} (Fig. 4A). There is a linear relationship between the anodic peak current, I_{pa}, and the cathodic peak current, I_{pc}, with the scan rate,

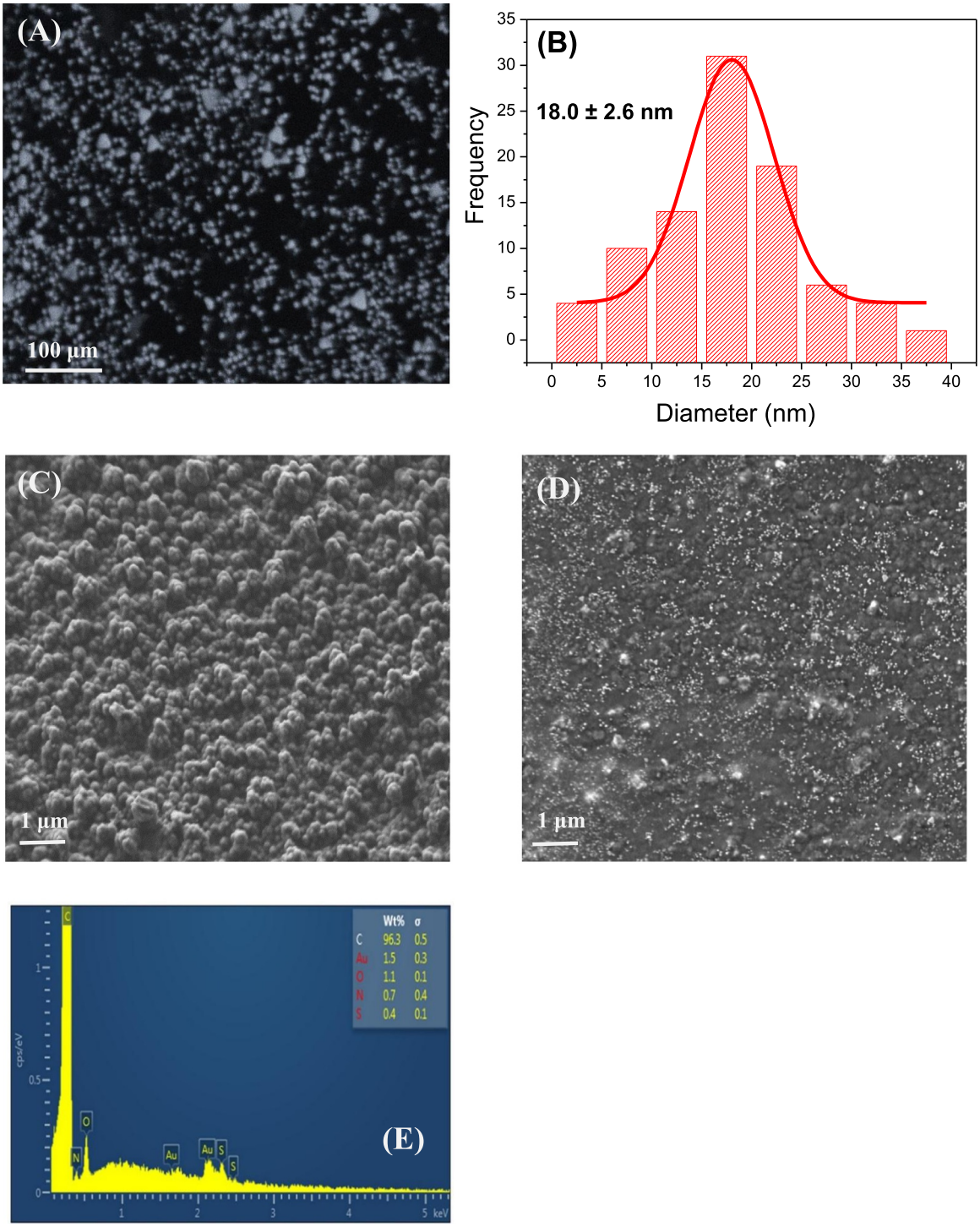

Fig. 2. (A) Scanning electron microscopy (SEM) of the gold nanoparticles (AuNP) obtained by green synthesis; (B) Size distribution histogram of the AuNP; (C) SEM of PANSA; (D) SEM of the AuNP-PANSA nanocomposite film; (E) EDS spectrum of the AuNP-PANSA nanocomposite film.

v, (Fig. 4B), according to the equations: I_{pa} (µA) = -0.24 v + 0.05; r = 0.9980 and I_{pc} (µA) = - 0.046 v – 0.33; r = 0.9985. characteristic of a surface-confined oxidation process [25]. A plot of the logarithm of the peak current vs logarithm of scan rate (not shown) has a slope of 1.12, close to the theoretical value of 1.0 for a pure adsorption controlled electrode reaction [25]. The same was observed at glassy carbon electrodes modified with AuNP-PANSA [19].

The current also depends on the amount of Tyr in solution which demonstrates that the adsorption is reversible and that the number of adsorbed species depends on the solution concentration, and that it can be described by an isotherm. When carrying out consecutive CV scans, a current decreasing with each scan was observed, since there was not time for the adsorption/desorption equilibrium of Tyr to be reached. In other experiments, after performing a scan in the presence of tyramine and then placing the electrode in pure buffer solution, the CV peak of tyramine oxidation appeared, also indicating that there is tyramine adsorbed on the modified electrode. The separation of the anodic and cathodic peaks increases with increasing scan rate, typical for a quasi-reversible process. The dependence of the anodic peak potential, E_{pa} and the cathodic peak potential, E_{pc}, on the logarithm of scan rate are

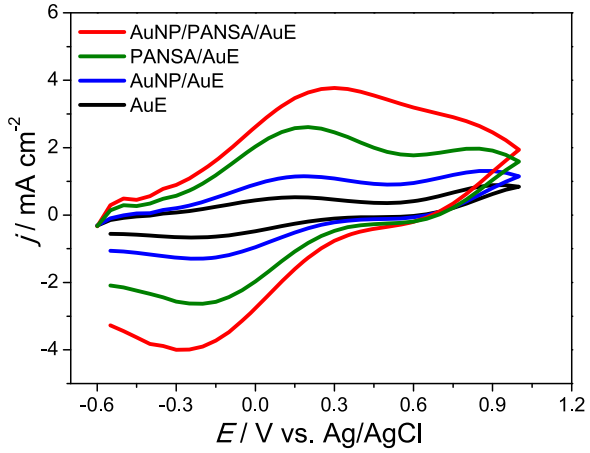

Fig. 3. Cyclic voltammograms for the oxidation of 200 µM Tyr in 0.1 M BR buffer solution (pH 7.0), recorded at 50 mV s^{-1}, at (▬) AuE; (▬) AuNP/AuE; (▬) PANSA/AuE; (▬) AuNP-PANSA/AuE.

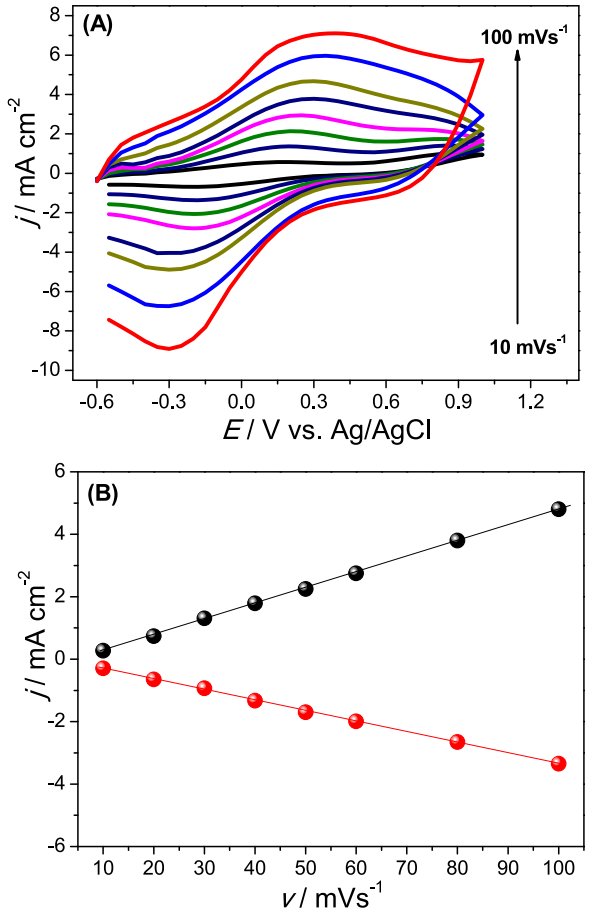

Fig. 4. (A) Cyclic voltammograms at AuNP-PANSA/AuE in 200 µM Tyr solution (0.1 M BR buffer, pH 7.0) at scan rates 10–100 mV s^{-1}. (B) The linear relationship between the peak currents and scan rate.

given by Laviron's equations for anodic and cathodic processes [26]:

$$E_{pa} = \left(\frac{2.303RT}{\alpha_a nF}\right)\log v + K \qquad E_{pc} = \left(\frac{-2.303RT}{\alpha_c nF}\right)\log v + K$$

where α_a and α_c are the anodic and cathodic electron transfer coefficients, n is the number of electrons involved in the redox process, F is the Faraday constant (F = 96485 C mol^{-1}), v is the potential scan rate (V s^{-1}), R is the ideal gas constant (8.314 J K^{-1} mol^{-1}), T is the temperature (K) and K is a constant. The dependence between the peak potential and logarithm of scan rate are expressed as: E_{pa} (V) = 0.084 $\log v$ + 0.094 and E_{pc} (V) = - 0.065 $\log v$ - 0.10. Taking into account the two-electron process for Tyr oxidation [27], the charge transfer coefficients were estimated to be α_a = 0.40 and α_c = 0.54.

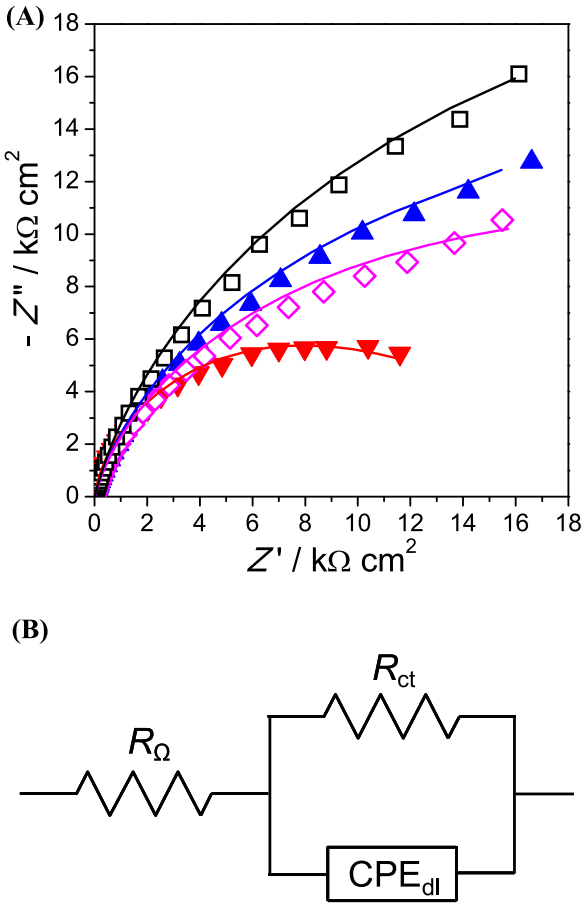

Fig. 5. (A) Complex plane impedance spectra recorded at different electrode configurations: (□) AuE; (▲) AuNP/AuE; (◇) PANSA/AuE; (▼) AuNP-PANSA/AuE in the presence of 100 µM tyramine in 0.1 M BR buffer (pH 7.0) at 0.6 V vs. Ag/AgCl. (B) Electrical equivalent circuit used to fit the impedance spectra: R_Ω cell resistance; CPE_{dl} non-ideal capacitance of the double layer; R_{ct} charge transfer resistance.

3.4.2. *Electrochemical impedance spectroscopy (EIS)*

EIS is a powerful analytical tool for analysing the complex electrochemical properties of a system and is very sensitive for sensor applications. Impedance spectra can be analysed by fitting to an equivalent electrical circuit to obtain the values of the electrical components which model each interfacial phenomenon, thus permitting the elucidation of the processes of charge transfer and charge separation [28].

Impedance spectra were recorded at AuNP-PANSA/AuE at different potentials from 0.0 to + 0.8 V, chosen as explained below in Section 3.5.1. Impedance spectra at + 0.6 V, the best potential for impedimetric detection as will be shown below, for different electrode configurations AuE, AuNP/AuE, PANSA/AuE, AuNP-PANSA/AuE are shown in Fig. 5A.

All spectra showed a semicircle–like shape and were fitted with the same electrical equivalent circuit presented in Fig. 5B. Although it is expected that the circuit should contain contributions from the modifier film resistance and capacitance as well as from the modified electrode-solution interface, the experimental spectra are clearly dominated by one *RC* parallel combination with no other semicircles with different time constants discernible, as usually happens. Thus, the circuit

Table 1
Values of equivalent circuit parameters obtained by fitting of the impedance spectra at different electrode configurations; + 0.6 V (0.1 M BR buffer, pH 7.0). Data from Fig. 5A.

Electrode configuration	R_{ct}/ kΩ cm^2	CPE_{dl} / μF cm^{-2} s$^{\alpha-1}$	α
AuE	34.4	27.3	0.84
AuNP/AuE	25.8	31.9	0.84
PANSA/AuE	20.9	35.1	0.85
AuNP-PANSA/AuE	10.8	44.7	0.90

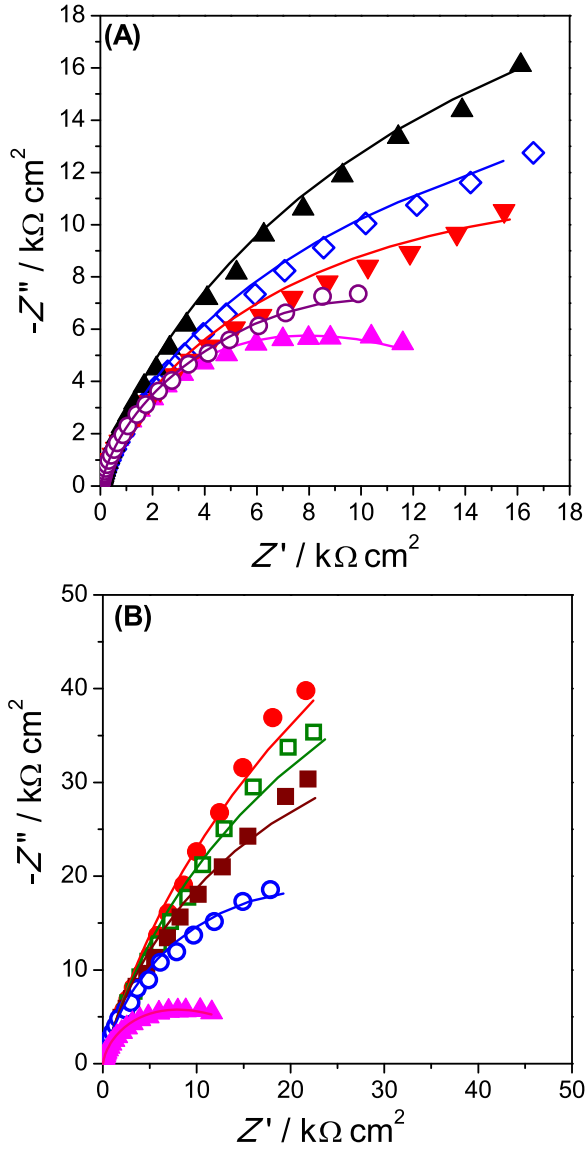

Fig. 6. Complex plane impedance spectra at AuNP-PANSA/AuE in the presence of 100 μM Tyr in 0.1 M BR buffer (A) At pH 7.0, applied potential (◇) 0.0; (▲) 0.2; (▼) 0.4; (▲) 0.6; (○) 0.8 V vs. Ag/AgCl. (B) At + 0.6 V vs. Ag/AgCl, pH values of (●) 4.0; (□) 5.0; (■) 6.0; (▲) 7.0; (○) 8.0.

comprises R_Ω, the cell resistance (solution resistance, electrical contacts etc.) in series with a parallel combination of R_{ct} and CPE_{dl}, representing the charge transfer resistance and non-ideal interfacial capacitance respectively. The CPE is modelled as a non-ideal capacitor given by $CPE = -1/(i\omega C)^{\alpha}$ in which the exponent α reflects the surface non-uniformity and roughness of the modified electrode assembly, where $\alpha = 1$ corresponds to a perfect uniform and smooth surface [29,30]. The results from fitting to the equivalent circuit are summarized in Table 1 and are shown as continuous curves in the spectra.

Table 2
Equivalent circuit element values obtained by fitting of the impedance spectra at AuNP-PANSA/AuE at different potentials (pH 7.0, data from Fig. 6A) and different pH values (+0.6 V, data from Fig. 6B).

Experimental conditions		R_{ct} / kΩ cm^2	CPE_{dl} / μF cm^{-2} s$^{\alpha-1}$	α
Applied potential / V	0.0	53.2	19.3	0.85
	0.2	103.4	20.8	0.84
	0.4	84.4	18.4	0.85
	0.6	15.8	19.2	0.90
	0.8	30.7	25.0	0.88
pH	4.0	170.2	19.7	0.85
	5.0	121.3	19.9	0.83
	6.0	70.5	19.6	0.85
	7.0	15.8	19.2	0.90
	8.0	45.8	19.8	0.86

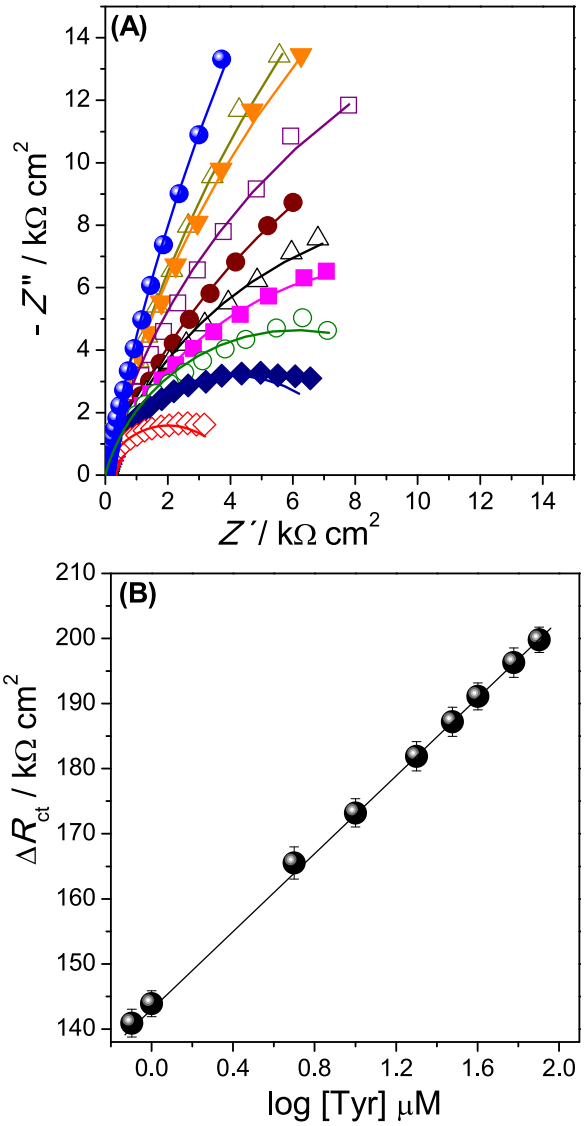

Fig. 7. (A) Complex plane impedance spectra at AuNP-PANSA/AuE with different concentrations of Tyr in 0.1 M BR buffer (pH 7.0) at 0.6 V vs. Ag/AgCl: (●) 0.0; (△) 0.8; (▼) 1.0; (□) 5.0; (●) 10.0; (Δ) 20.0; (■) 30.0; (○) 40.0; (◆) 60.0; (◇) 80.0 μM. (B). Calibration curve of ΔR_{ct} versus log ([Tyr]/μM).

The EIS data show that the double layer capacitance increases with modification of the electrode reaching a maximum at the AuNP-PANSA modified electrode. The increase in the capacitance values is accompanied by the decrease in the charge transfer resistance values. A higher

Table 3
Equivalent circuit element values obtained by fitting of the impedance spectra at AuNP-PANSA/AuE with different Tyr concentrations. Data from Fig. 7.

[Tyramine] / μM	R_{ct} / kΩ cm^2	CPE_{dl} / μF cm^{-2} s$^{\alpha-1}$	α
0.0	204	18.0	0.87
0.8	63.1	22.3	0.88
1.0	49.1	38.2	0.89
5.0	31.5	42.6	0.89
10	25.8	45.5	0.86
20	16.1	57.8	0.85
30	13.8	63.6	0.84
40	10.9	72.9	0.85
60	7.7	75.3	0.90
80	4.2	84.9	0.89

value of the exponent α equal to 0.90 was obtained for AuNP-PANSA/AuE indicating that it has a more uniform surface at the nanoscale compared to the other electrode configurations, as also verified by SEM morphological studies. The R_{ct} values of the modified electrodes of 34.4, 25.8, 20.9 and 10.8 kΩ cm^2 decrease in the order AuE, AuNP/AuE, PANSA/AuE, AuNP-PANSA/AuE, respectively, indicating the easiest electron transfer at the last electrode configuration. This can be explained considering a synergetic effect of nanoparticles and polymer, which leads to an increase of electroactive area and contributes to an electrocatalytic effect towards tyramine. The impedance spectra are in agreement with the cyclic voltammetry observations.

3.5. Optimization of the working conditions for Tyr determination

3.5.1. Influence of the applied potential

For electrochemical impedimetric as well as voltammetric measurements, the applied potential has a big influence on sensor response since it contributes to a better sensitivity for detection of the target analyte. In order to optimize the potential for detection of Tyr, impedance spectra were recorded at different potentials: 0.0, 0.2, 0.4, 0.6 and 0.8 V vs. Ag/AgCl. These potentials were chosen considering the oxidation peak potential values from CV and encompass the range of potentials where oxidation and reduction occur. Moreover, using potentials as close as possible to 0.0 V should minimise interference effects.

Fig. 6A shows impedance spectra recorded at AuNP-PANSA/AuE in the presence of 100 μM Tyr in BR buffer solution, pH 7.0 at the various potentials. Table 2 shows the results of fitting the data to the electrical equivalent circuit in Fig. 5B, where it can be observed that the lowest values of R_{ct} are obtained at 0.6 V, in agreement with CV results, where the maximum oxidation peak appears around 0.55 V, Fig. 4A. Therefore, 0.6 V was taken as the best value for Tyr determination by impedance.

3.5.2. Influence of the solution pH

The effect of supporting electrolyte pH on the spectra was investigated to evaluate the optimum pH for determination of Tyr. Spectra were recorded, as shown in Fig. 6B, in the presence of 100 μM Tyr in BR buffer at the pH range from 4.0 to 8.0 at AuNP-PANSA/AuE at + 0.6 V. As can be seen from Table 2, the values of R_{ct} gradually decreased with increase of pH up to pH 7, then increased. The fact that R_{ct} decreases with increase of pH may reflect the lower stability of the chemical equilibrium dopamine-o-quinone by-products formed during oxidation of Tyr in acid and basic pH solution, giving a better response at neutral pH [31].

3.6. Impedimetric response for Tyr determination

Impedance spectra recorded under the optimum conditions determined above for Tyr sensing are shown as complex plane plots in Fig. 7A, for concentrations up to 80.0 μM. It is possible to observe a change in the shape of the spectra, associated with a decrease in the R_{ct} value, immediately with the first concentration of Tyr added, and this can be associated with a realistic limit of detection. The errors associated with fitting to electrical circuit were less than 3% and the changes in R_{ct} were much higher than this. The values of the equivalent circuit parameters after fitting the spectra are summarized in Table 3. It is clearly seen that R_{ct} decreases with increase of Tyr concentration, while the capacitance values gradually increase.

The calibration curve in Fig. 7B plots the change of charge transfer resistance ΔR_{ct} ($R_{ct(buffer)} - R_{ct(tyr)}$) versus log [Tyr] according to the equation ΔR_{ct} (kΩ) = 144.1 + 29.4 (log[C/μM]) with a correlation coefficient of 0.9987. The reason for the logarithmic dependence can be attributed to the adsorption of Tyr's oxidation product on the electrode surface. The detection limit was calculated to be 0.04 μM based on three replicates. The good performance of the novel Tyr impedimetric sensor considering its ease of fabrication and simplicity of architecture is mainly attributed to a high area-volume ratio, excellent conducting capability and interface-dominated properties of AuNP, which, in combination with the properties of the PANSA polymer network, provide an effective modifier for Tyr oxidation.

The analytical performance of the nanocomposite AuNP-PANSA/AuE for Tyr determination was compared with other electrode configurations (no reports on impedimetric sensing were found) and the results are listed in Table 4. The novel impedimetric sensor used for Tyr detection showed a superior performance to those found in the literature with the lowest limit of detection and a sufficiently broad linear range, comparable to more complex architectures that use carbon nanotubes and/or tyrosinase.

Although in some configurations tyrosinase was used [32,33], with Tyr as enzyme substrate, their performance was not better than here. The sensors that used DPV for analytical Tyr determination [27,34] presented a higher limit of detection despite the high sensitivity conferred by DPV. This can be attributed to the accentuated adsorption that compromises the detection by voltammetric techniques, as verified in previous studies [27,32–35]. Hence, the proposed novel nanocomposite with impedimetric measurement has the advantage of easy and rapid preparation with very low limit of detection.

Table 4
Comparison of the tyramine determination performance at AuNP-PANSA/AuE with different electrode configurations in the literature.

Modified electrode configuration	Principle of detection	pH, buffer	Linear range / μM	LOD / μM	Ref
Q/fMWCNT/GCE	DPV	7.0, PBS (0.1 M)	0.7–75	0.65	[27]
Carbon disc	MECC-AD	10.3, borate-NaOH (0.02 M)	1–1000	0.18	[35]
fMWCNT/GCE	DPV	7.0, PBS (0.1 M)	1–17	0.80	[34]
Tyrosinase/PPy/PtE	Amperometry	7.0, PBS (0.01 M)	4–80	0.54	[32]
Tyrosinase/ COOfSWCNT	Amperometry	7.0, PBS (0.01 M)	5–180	0.62	[33]
AuNP-PANSA/AuE	EIS	7.0, BR (0.1 M)	0.8–80	0.04	This work

Q – quercetin; fMWCNT - functionalized multi-walled carbon nanotubes; GCE – glassy carbon electrodes; MECC-AD - micellar electrokinetic capillary chromatography separation with amperometric detection; DPV- Differential pulse voltammetry; PPy – polypyrrole; PtE – platinum electrode; COOfSWCNT – carboxyl functionalized single-walled carbon nanotubes; EIS – Electrochemical impedance spectroscopy.

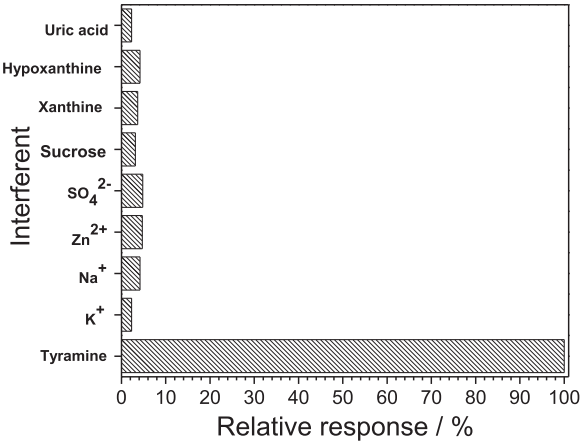

Fig. 8. Influence of potential interferents on the impedimetric sensor response in the presence of 100 μM Tyr, ratio with interferents (1:1).

Table 5
Determination of tyramine in fermented drink and dairy products.

Sample	Determined (μM)	Added (μM)	Expected (μM)	Found (μM)	RSD (%)	Recovery (%)
Roquefort cheese	4.36	2.00	6.36	6.28	2.16	98.7
Yogurt	0.18	2.00	2.18	2.13	4.79	97.7
Red wine	1.58	2.00	3.58	3.51	3.18	98.0
Beer	1.69	2.00	3.69	3.76	4.12	101.9

3.7. Repeatability, stability, and selectivity

The repeatability of impedimetric measurements at the AuNP-PANSA/AuE was investigated by successive measurements of the response to 100 μM Tyr in buffer BR, pH 7.0. The R_{ct} value was 95% of the initial value after 25 successive measurements (RSD = 4.39%; n = 3). With respect to storage stability, the EIS response of the sensor lost just 10% of the initial signal in terms of the R_{ct} value, after a storage period of 20 days in the dry state at room temperature.

The influence of potential interferents on sensor response was evaluated. For this, the possible interferents tested were: organic (uric acid, hypoxanthine, xanthine, sucrose) and inorganic species (SO_4^{2-}, Zn^{2+}, Na^+, K^+) in the ratio 1:1(m/m) with Tyr and the results are shown in Fig. 8. As can be seen, these species did not produce significant changes in the R_{ct} values (all less than 5%), demonstrating good selectivity. This selectivity is comparable to that reported in the literature [36,37].

3.8. Determination of Tyr in commercial food products

The impedimetric sensor was applied to detect Tyr in food samples purchased from the local market: dairy products (Roquefort cheese and yogurt) and fermented drinks (red wine and beer). The analytical determination was performed using standard addition method and the values calculated based on average of three replicates are summarized in Table 5. The quantity of Tyr found in the original samples is given as the value obtained after dilution; in the case of the dairy foods by a factor of 20 and for fermented drinks 100 times dilution. The calculated amounts of Tyr found in Roquefort cheese and yogurt were 59.8 mg L^{-1} and 2.47 mg L^{-1} respectively. For the fermented drinks, it was 8.66 mg L^{-1} in red wine and 9.27 mg L^{-1} in beer samples. These values are in agreement with other work on this topic [38–40]. Recovery measurements gave values in the range from 97.7% to 101.9% with RSD values of less than 5.0%, indicating that the proposed sensor is useful for practical applications in food safety control.

4. Conclusions

A simple and inexpensive electrochemical impedimetric sensor for the detection of Tyr has been developed for the first time, based on a nanocomposite (polymer and gold nanoparticles) film modified gold electrode. Electrochemical impedance has been shown to be a very sensitive technique for the analytical determination of Tyr. The impedimetric sensor proposed possesses good selectivity, reproducibility, stability and high selectivity, with fast response and low limit of detection. It was successfully used for Tyr detection in dairy products and fermented drinks with good recoveries, which suggests its application to food monitoring.

Acknowledgements

The authors thank Fundaç ão para a Ciência e a Tecnologia (FCT), Portugal, projects PTDC/QEQ-QAN/2201/2014, in the framework of Project 3599-PPCDT, and UID/EMS/00285/2013 (both co-financed by the European Community Fund FEDER) and the European Union Marie Curie International Research Staff Exchange Scheme (IRSES), project SmartCancerSens PIRSES-GA-2012–318053, for financial support. MEG thanks FCT for a postdoctoral fellowship SFRH/BPD/103103/2014 and WS thanks the Conselho Nacional de Desenvolvimento Científico e Tecnológico (CNPq), Brazil for a doctoral fellowship.

References

[1] K.B. Narayanan, N. Sakthivel, Coriander leaf mediated biosynthesis of gold nanoparticles, Mater. Lett. 62 (2008) 4588–4590, https://doi.org/10.1016/J.MATLET.2008.08.044.
[2] A. Yassoralipour, J. Bakar, R.A. Rahman, F. Abu Bakar, Biogenic amines formation in barramundi (Lates calcarifer) fillets at 8 °C kept in modified atmosphere packaging with varied CO_2 concentration, LWT - Food Sci. Technol. 48 (2012) 142–146, https://doi.org/10.1016/J.LWT.2012.01.033.
[3] G. Tabanelli, F. Coloretti, C. Chiavari, L. Grazia, R. Lanciotti, F. Gardini, Effects of starter cultures and fermentation climate on the properties of two types of typical Italian dry fermented sausages produced under industrial conditions, Food Control. 26 (2012) 416–426, https://doi.org/10.1016/J.FOODCONT.2012.01.049.
[4] A.S. Hernández-Cázares, M.-C. Aristoy, F. Toldrá, An enzyme sensor for the determination of total amines in dry-fermented sausages, J. Food Eng. 106 (2011) 166–169, https://doi.org/10.1016/J.JFOODENG.2011.04.026.
[5] I. Al Bulushi, S. Poole, H.C. Deeth, G.A. Dykes, Biogenic amines in fish: roles in intoxication, spoilage, and nitrosamine formation-A review, Crit. Rev. Food Sci. Nutr. 49 (2009) 369–377, https://doi.org/10.1080/10408390802067514.
[6] A. Önal, S.E.K. Tekkeli, C. Önal, A review of the liquid chromatographic methods for the determination of biogenic amines in foods, Food Chem. 138 (2013) 509–515, https://doi.org/10.1016/j.foodchem.2012.10.056.
[7] V. Gianotti, U. Chiuminatto, E. Mazzucco, F. Gosetti, M. Bottaro, P. Frascarolo, M.C. Gennaro, A new hydrophilic interaction liquid chromatography tandem mass spectrometry method for the simultaneous determination of seven biogenic amines in cheese, J. Chromatogr. A. 1185 (2008) 296–300, https://doi.org/10.1016/J.CHROMA.2008.02.038.
[8] T. Lapainis, C. Scanlan, S.S. Rubakhin, J.V. Sweedler, A multichannel native fluorescence detection system for capillary electrophoretic analysis of neurotransmitters in single neurons, Anal. Bioanal. Chem. 387 (2007) 97–105, https://doi.org/10.1007/s00216-006-0775-9.
[9] V. Ladero, N. Martínez, M.C. Martín, M. Fernández, M.A. Alvarez, qPCR for quantitative detection of tyramine-producing bacteria in dairy products, Food Res. Int. 43 (2010) 289–295, https://doi.org/10.1016/j.foodres.2009.10.007.
[10] M.F.S. Teixeira, M.F. Bergamini, C.M.P. Marques, N. Bocchi, Voltammetric determination of L-dopa using an electrode modified with trinuclear ruthenium ammine complex (Ru-red) supported on Y-type zeolite, Talanta 63 (2004) 1083–1088, https://doi.org/10.1016/j.talanta.2004.01.018.
[11] S. Shahrokhian, E. Asadian, Electrochemical determination of l-dopa in the presence of ascorbic acid on the surface of the glassy carbon electrode modified by a bilayer of multi-walled carbon nanotube and poly-pyrrole doped with tiron, J. Electroanal. Chem. 636 (2009) 40–46, https://doi.org/10.1016/j.jelechem.2009.09.010.
[12] O. Tovide, N. Jaheed, N. Mohamed, E. Nxusani, C.E. Sunday, A. Tsegaye, R.F. Ajayi, N. Njomo, H. Makelane, M. Bilibana, P.G. Baker, A. Williams, S. Vilakazi, R. Tshikhudo, E.I. Iwuoha, Graphenated polyaniline-doped tungsten oxide nanocomposite sensor for real time determination of phenanthrene, Electrochim. Acta 128 (2014) 138–148, https://doi.org/10.1016/j.electacta.2013.12.134.
[13] O. Tovide, N. Jahed, C.E. Sunday, K. Pokpas, R.F. Ajayi, H.R. Makelane, K.M. Molapo, S.V. John, P.G. Baker, E.I. Iwuoha, Electro-oxidation of anthracene on polyanilino-graphene composite electrode, Sensors Actuators, B Chem. 205 (2014) 184–192, https://doi.org/10.1016/j.snb.2014.07.116.

[14] R.F. Ngece, N. West, P.M. Ndangili, R.A. Olowu, A. Williams, N. Hendricks, S. Mailu, P. Baker, E. Iwuoha, A silver nanoparticle/poly (8-Anilino-1-naphthalene Sulphonic acid) bioelectrochemical biosensor system for the analytical determination of ethambutol, Int. J. Electrochem. Sci. 6 (2011) 1820–1834.
[15] H. Bhandari, V. Choudhary, S.K. Dhawan, Influence of self-doped poly(aniline-co-4-amino-3-hydroxy-naphthalene-1- sulfonic acid) on corrosion inhibition behaviour of iron in acidic medium, Synth. Met. 161 (2011) 753–762, https://doi.org/10.1016/j.synthmet.2011.01.026.
[16] M.M. Barsan, C.M.A. Brett, Recent advances in layer-by-layer strategies for biosensors incorporating metal nanoparticles, TrAC, Trends Anal. Chem. 79 (2015) 286–296, https://doi.org/10.1016/j.trac.2015.11.019.
[17] H. Hosseini, M. Behbahani, M. Mahyari, H. Kazerooni, A. Bagheri, A. Shaabani, Ordered carbohydrate-derived porous carbons immobilized gold nanoparticles as a new electrode material for electrocatalytical oxidation and determination of nicotinamide adenine dinucleotide, Biosens. Bioelectron. 59 (2014) 412–417, https://doi.org/10.1016/j.bios.2014.02.046.
[18] A. Ananthi, K.L. Phani, Self-assembly of gold nanoparticles on sulphide functionalized polydopamine in application to electrocatalytic oxidation of nitric oxide, J. Electroanal. Chem. 764 (2016) 7–14, https://doi.org/10.1016/j.jelechem.2016.01.003.
[19] W. da Silva, M.E. Ghica, R.F. Ajayi, E.I. Iwuoha, C.M.A. Brett, Tyrosinase based amperometric biosensor for determination of tyramine in fermented food and beverages with gold nanoparticle doped poly(8-anilino-1-naphthalene sulphonic acid) modified electrode. [Submitted], Food Chem, 2018.
[20] M.V. Sujitha, S. Kannan, Green synthesis of gold nanoparticles using Citrus fruits (Citrus limon, Citrus reticulata and Citrus sinensis) aqueous extract and its characterization, Spectrochim. Acta - Part A Mol. Biomol. Spectrosc. 102 (2013) 15–23, https://doi.org/10.1016/j.saa.2012.09.042.
[21] R. Mažeikiene, G. Niaura, A. Malinauskas, Raman spectroelectrochemical study of self-doped copolymers of aniline and selected aminonaphthalenesulfonates, Electrochim. Acta 51 (2006) 1917–1924, https://doi.org/10.1016/j.electacta.2005.06.025.
[22] P. Khademi-Azandehi, J. Moghaddam, Green synthesis, characterization and physiological stability of gold nanoparticles from Stachys lavandulifolia Vahl extract, Particuology 19 (2015) 22–26, https://doi.org/10.1016/j.partic.2014.04.007.
[23] F.U. Khan, Y. Chen, N.U. Khan, A. Ahmad, K. Tahir, Z.U.H. Khan, A.U. Khan, S.U. Khan, M. Raza, P. Wan, Visible light inactivation of E. coli, Cytotoxicity and ROS determination of biochemically capped gold nanoparticles, Microb. Pathog. 107 (2017) 419–424, https://doi.org/10.1016/j.micpath.2017.04.024.
[24] A.K. Suresh, D.A. Pelletier, W. Wang, M.L. Broich, J.W. Moon, B. Gu, D.P. Allison, D.C. Joy, T.J. Phelps, M.J. Doktycz, Biofabrication of discrete spherical gold nanoparticles using the metal-reducing bacterium Shewanella oneidensis, Acta Biomater. 7 (2011) 2148–2152, https://doi.org/10.1016/j.actbio.2011.01.023.
[25] C. Brett, A. Brett, Electrochemistry: principles, methods, and applications, Springer, 1993, p. 427, https://doi.org/10.1002/anie.199419892.
[26] E. Laviron, General expression of the linear potential sweep voltammogram in the case of diffusionless electrochemical systems, J. Electroanal. Chem. 101 (1979) 19–28, https://doi.org/10.1016/S0022-0728(79)80075-3.
[27] J.B. Raoof, R. Ojani, M. Amiri-Aref, M. Baghayeri, Electrodeposition of quercetin at a multi-walled carbon nanotubes modified glassy carbon electrode as a novel and efficient voltammetric sensor for simultaneous determination of levodopa, uric acid and tyramine, Sens. Actuators, B Chem. 166–167 (2012) 508–518, https://doi.org/10.1016/j.snb.2012.02.096.
[28] D. Chan, M.M. Barsan, Y. Korpan, C.M.A. Brett, L-lactate selective impedimetric bienzymatic biosensor based on lactate dehydrogenase and pyruvate oxidase, Electrochim. Acta 231 (2017) 209–215, https://doi.org/10.1016/j.electacta.2017.02.050.
[29] M.E. Ghica, C.M.A. Brett, Poly(brilliant cresyl blue) modified glassy carbon electrodes: electrosynthesis, characterisation and application in biosensors, J. Electroanal. Chem. 629 (2009) 35–42, https://doi.org/10.1016/j.jelechem.2009.01.019.
[30] D.R. Kumar, S. Kesavan, M.L. Baynosa, J.-J. Shim, 3,5-Diamino-1,2,4-triazole@ electrochemically reduced graphene oxide film modified electrode for the electrochemical determination of 4-nitrophenol, Electrochim. Acta 246 (2017), https://doi.org/10.1016/j.electacta.2017.06.116.
[31] M. Cheng, X. Zhang, M. Wang, H. Huang, J. Ma, A facile electrochemical sensor based on well-dispersed graphene-molybdenum disulfide modified electrode for highly sensitive detection of dopamine, J. Electroanal. Chem. 786 (2017) 1–7, https://doi.org/10.1016/j.jelechem.2017.01.012.
[32] I.M. Apetrei, C. Apetrei, Amperometric biosensor based on polypyrrole and tyrosinase for the detection of tyramine in food samples, Sens. Actuators, B Chem. 178 (2013) 40–46, https://doi.org/10.1016/j.snb.2012.12.064.
[33] I.M. Apetrei, C. Apetrei, The biocomposite screen-printed biosensor based on immobilization of tyrosinase onto the carboxyl functionalised carbon nanotube for assaying tyramine in fish products, J. Food Eng. 149 (2015) 1–8, https://doi.org/10.1016/j.jfoodeng.2014.09.036.
[34] J.B. Raoof, R. Ojani, M. Baghayeri, M. Amiri-Aref, Application of a glassy carbon electrode modified with functionalized multi-walled carbon nanotubes as a sensor device for simultaneous determination of acetaminophen and tyramine, Anal. Methods 4 (2012) 1579–1587, https://doi.org/10.1039/C2ay05494a.
[35] Q. Wang, H. Yu, H. Li, F. Ding, P. He, Y. Fang, Simultaneous determination of food-related biogenic amines and precursor amino acids by micellar electrokinetic capillary chromatography with electrochemical detection, Food Chem. 83 (2003) 311–317, https://doi.org/10.1016/S0308-8146(03)00223-1.
[36] J. Huang, X. Xing, X. Zhang, X. He, Q. Lin, W. Lian, H. Zhu, A molecularly imprinted electrochemical sensor based on multiwalled carbon nanotube-gold nanoparticle composites and chitosan for the detection of tyramine, Food Res. Int. 44 (2011) 276–281, https://doi.org/10.1016/j.foodres.2010.10.020.
[37] Y. Li, C.H. Hsieh, C.W. Lai, Y.F. Chang, H.Y. Chan, C.F. Tsai, J.-an A. Ho, L. chen Wu, Tyramine detection using PEDOT:PSS/AuNPs/1-methyl-4-mercaptopyridine modified screen-printed carbon electrode with molecularly imprinted polymer solid phase extraction, Biosens. Bioelectron. 87 (2017) 142–149, https://doi.org/10.1016/j.bios.2016.08.006.
[38] J.L. Ordóñez, A.M. Troncoso, M.D.C. García-Parrilla, R.M. Callejón, Recent trends in the determination of biogenic amines in fermented beverages – A review, Anal. Chim. Acta 939 (2016) 10–25, https://doi.org/10.1016/j.aca.2016.07.045.
[39] A.M.C.V.-C.S. Novella-Rodríguez, M.T. Veciana-Nogués, M. Izquierdo-Pulido, Distribution of biogenic amines and polyamines in cheese, J. FOOD Sci. 68 (2003) 750–755, https://doi.org/10.1111/j.1365-2621.2003.tb08236.x.
[40] C.M. Mayr, P. Schieberle, Development of stable isotope dilution assays for the simultaneous quantitation of biogenic amines and polyamines in foods by LC-MS/MS, J. Agric. Food Chem. 60 (2012) 3026–3032, https://doi.org/10.1021/jf204900v.